J Mater Sci: Mater Med (2007) 18:111–118
DOI 10.1007/s10856-006-0668-7

Annealing study of palladium–silver dental alloys: Vickers hardness measurements and SEM microstructural observations

W. H. Guo · W. A. Brantley · D. Li · W. A. T. Clark · P. Monaghan · R. H. Heshmati

Received: 27 September 2005 / Accepted: 14 November 2005

Abstract Three Pd–Ag dental alloys for metal-ceramic restorations, W-1 (Ivoclar Vivadent), Rx 91 (Pentron) and Super Star (Heraeus Kulzer), were subjected to isothermal annealing for 0.5 hr periods in a nitrogen atmosphere at temperatures from approximately 400° to 950°C. The annealing behavior was investigated by Vickers hardness measurements (1 kg load) and SEM microstructural observations. The highest Vickers hardness occurred at approximately 700°C for W-1 and 650°C for Rx 91. For Super Star, there were two peaks in hardness at approximately 500° and 650°C. Additional use of light indenting loads (25 g for W-1; 10 g for Rx 91 and Super Star) revealed that hardness variations during annealing for W-1 and Rx 91 were related to the palladium solid solution matrix phase. For Super Star, the lower-temperature peak was controlled by multi-phase regions and the higher-temperature peak by the matrix phase. While microstructural changes due to annealing were evident with the SEM for Rx 91 and Super Star, no correlation was possible for W-1 because of its finer-scale microstructure. Although commercial Pd–Ag alloys have a relatively narrow composition range, their microstructures and annealing behavior can vary because of differences in proportions of secondary elements utilized for porcelain adherence and grain refinement elements, as well as other proprietary strategies employed by the manufacturers.

W. H. Guo · W. A. Brantley · P. Monaghan · R. H. Heshmati
Section of Restorative and Prosthetic Dentistry, College of Dentistry, The Ohio State University, Columbus, OH, USA

D. Li
Section of Oral Biology, College of Dentistry, The Ohio State University, Columbus, OH, USA

W. A. T. Clark
Department of Materials Science and Engineering, The Ohio State University, Columbus, OH, USA

W. H. Guo
Center for Biological and Environmental Nanotechnology (CBEN), Rice University, Houston, TX, USA

P. Monaghan
Sherman Dental Associates, Evanston, IL

W. A. Brantley (✉)
Section of Restorative and Prosthetic Dentistry, College of Dentistry, The Ohio State University, PO Box 182357, Columbus, OH, USA 43218-2357
e-mail: brantley.1@osu.edu

1 Introduction

Palladium–silver alloys were first introduced for dental restorations in the 1970's as an alternative to costly gold-based dental alloys [1, 2]. The Pd–Ag alloys have the highest elastic modulus and sag resistance during porcelain firing of all noble metal dental casting alloys, excellent porcelain-metal bonding, favorable handling characteristics, ease of soldering, and satisfactory tarnish and corrosion resistance [3–7]. The commercially important alloys have a relatively narrow composition range, generally containing approximately 50%–60% Pd, 30%–40% Ag, and small amounts of Sn and In for porcelain bonding. The latter lower-melting point elements may also provide improved fluidity to the molten alloy and thus enhance castability. Because the original problem of porcelain greening discoloration by these alloys has been largely eliminated [3, 8, 9], the Pd–Ag alloys have become more popular than high-palladium alloys for metal–ceramic restorations, due to the recent price volatility of palladium.

Although palladium and silver form a solid solution system, non-equilibrium phases and microsegregation exist

in the rapidly solidified as-cast dental Pd–Ag alloys, and precipitates are found after the porcelain-firing heat-treatment because of the Sn and In components in the alloy composition [10, 11]. Mackert *et al.* [12] investigated the behavior of the W-1 Pd–Ag dental alloy (Ivoclar Vivadent, Amherst, NY, USA) during the initial oxidation procedure before porcelain firing and found that Pd–Ag nodules formed on the surface due to the internal oxidation of Sn and In. Payan *et al.* [13], subsequently found that the hardness of an experimental 59.3Pd–29.6Ag–8.8Sn–2.2In (wt.%) dental alloy varied with annealing from 400° to 1000°C, attaining a maximum value at 650°C. Since the alloy was annealed in air, they concluded that the hardness variations resulted from the internal oxidation of Sn and In that had been reported by Mackert *et al.* [12].

Our previous investigation of the Super Star Pd–Ag dental alloy (Heraeus Kulzer, Armonk, NY, USA) [11] revealed that discontinuous precipitates occurred in the matrix phase during porcelain-firing heat treatment. The aim of this study was to investigate hardness variations and microstructures for three clinically popular Pd–Ag dental alloys subjected to annealing heat treatments over a wide temperature range, and gain insight into the relationships between precipitation processes and hardness changes.

2 Materials and methods

Three representative Pd–Ag dental alloys (W-1, Rx 91, and Super Star) were selected for study. Nominal alloy compositions and nominal values of 0.2% yield strength (YS) [also termed proof stress] and percentage elongation at fracture for tensile loading and the simulated porcelain-firing heat-treated condition are listed in Table 1. A minimum value of 250 MPa for the latter is required in the current version of American Dental Association Specification No. 38 for casting alloys used in metal-ceramic restorations.

Preparation of cast specimens followed previously described procedures [14]. Wax patterns simulated a coping for a maxillary central incisor restoration, and castings were obtained with the use of a fine-grained, carbon-free, phosphate-bonded investment (Cera-Fina, Whip Mix Corp., Louisville, KY, USA). The alloys were melted with a multi-orifice gas-oxygen torch, centrifugally cast in a broken-arm casting machine (Sybron/Kerr, Romulus, MI, USA), and bench cooled. After divesting, castings were cross-sectioned into specimens having approximate dimensions 1.5 mm × 4 mm × 5 mm, using a low-speed, water-cooled diamond saw (Leco, St. Joseph, MI, USA).

Isothermal annealing was performed on individual specimens for 30-min time periods at temperatures from 400° to 950°C (with 50°C step intervals), using a nitrogen atmosphere. These temperatures encompass the normal range for the dental porcelain firing cycles. Subsequent to the annealing experiments, the furnace temperatures were corrected with a thermocouple to yield the actual annealing temperatures given in the figures to follow. After annealing, each specimen was resin-mounted, ground and polished using a standard sequence of metallographic abrasives. Following final polishing with 0.05 μm alumina slurries, specimens were etched in aqua region solutions having the composition of $1HNO_3 : 3HCl : 5H_2O$ (volume ratio). After sputter-coating with a thin Au—Pd film, etched microstructures were examined with an SEM (JSM-820, JEOL, Tokyo, Japan) at a range of magnifications.

The bulk Vickers hardness of each alloy after each annealing step was measured with an indenting force of 1 kg and loading time of 30 seconds. A lighter indenting force was used to obtain microhardness measurements of individual single-phase and multi-phase regions. The force magnitude was dependent on dimensions of the microstructural constituents, and a loading time of 30 seconds was again used. For Super Star and Rx 91, the small dimensions of the multi-phase regions necessitated an indenting force of 10 g, and lengths of the diagonals of the indentations were measured with the SEM. For W-1, the multi-phase and single-phase regions were sufficiently large that 25 g was used, and the lengths of the diagonals of the indentations were measured with the optical microscope attached to the hardness tester. Generally, 10 indentations were utilized to obtain values of bulk hardness and hardness of the separate microstructural constituents for each alloy at each annealing temperature.

3 Results

3.1 Hardness vs. annealing temperatures

The bulk Vickers hardness and the hardness of individual microstructural regions as a function of annealing temperature are presented in Fig. 1 for the three Pd–Ag alloys, where mean values and standard deviations are provided.

Figure 1 (a) shows that the bulk hardness of W-1 reached its highest value at an annealing temperature of approximately 700°C. Hardness variations with annealing temperature for the single-phase palladium solid solution matrix were consistent with those for the bulk alloy. The annealing heat treatments had minimal effect on the hardness of the multi-phase interdendritic regions, showing that the bulk hardness changes for this alloy after annealing were mainly controlled by changes in the matrix phase. It can also be seen in Fig. 1 (a) that the bulk hardness for the W-1 alloy was greater than individual values of hardness for the matrix and the interdendritic regions.

The Rx 91 alloy had the same trend in hardness variations as W-1, which would be expected from their nearly identical compositions (Table 1), although bulk hardness values were higher for Rx 91. Figure 1 (b) shows that the bulk hardness of

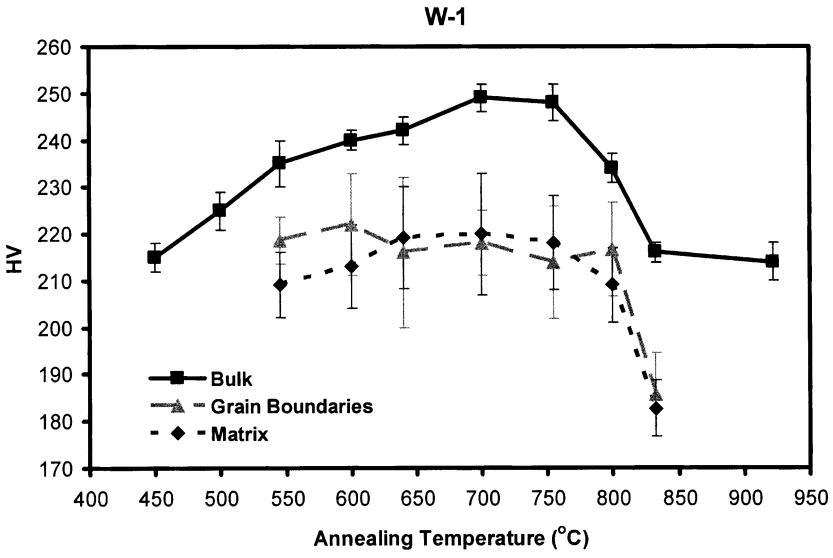

(a)

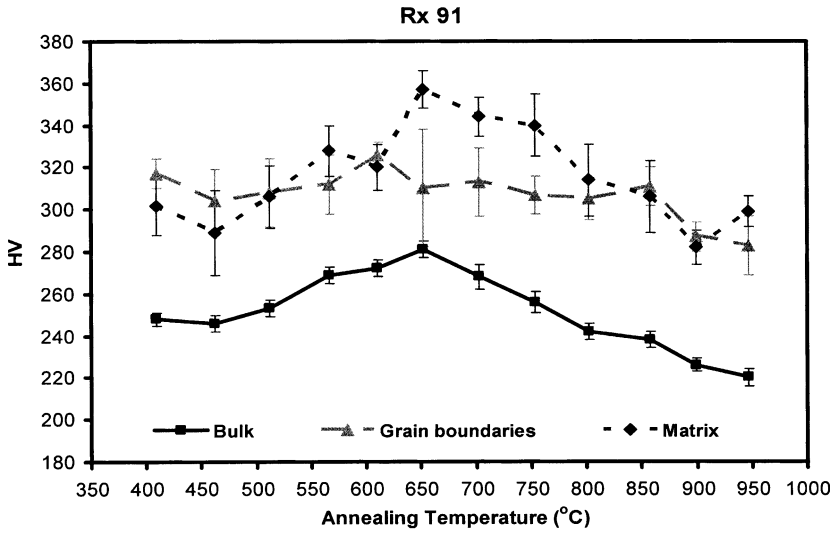

(b)

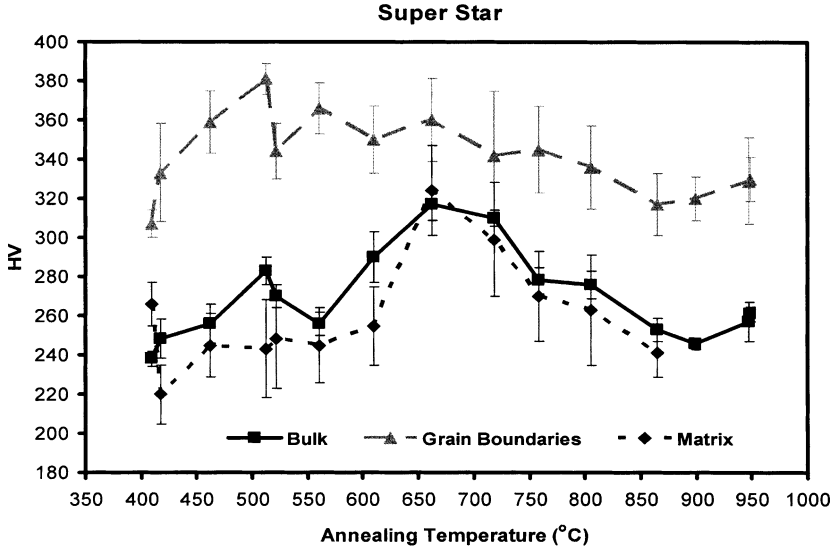

(c)

Fig. 1 Vickers hardness as function of annealing temperature for (a) W-1, (b) Rx 91, and (c) Super Star.

Table 1 Nominal compositions (wt.%) and mechanical properties reported by the manufacturers for the three Pd–Ag dental alloys studied

Alloy	Pd	Ag	Sn	In	Balance	0.2% YS (MPa)	Vickers Hardness	Elongation (%)
W-1*	53.3	37.7	8.5	<1	Ru, Li each < 1	485	240	11
Rx 91†	53.5	37.5	8.5	<1	Ru < 1	660	235	14
Super Star‡	59.8	28.1	5.0	6.0	Ga, Ru, Re each < 1	655	285	15

Note: Values for 0.2% yield strength, Vickers hardness and percentage elongation correspond to the simulated porcelain-firing heat-treated condition.
*Ivoclar Vivadent, Amherst, NY, USA. [Website: www.ivoclarvivadent.us.com]
†Pentron, Wallingford, CT, USA. [Website: www.pentron.com/pentron]
‡Heraeus Kulzer, Armonk, NY, USA. [Website: www.heraeus-kulzer-us.com]

Rx 91 had a maximum value at an annealing temperature of approximately 650°C. As with W-1, values of hardness for the palladium solid solution matrix in Rx 91 varied with annealing temperature in the same manner as the bulk hardness, and no meaningful variations in hardness caused by annealing were detected for the grain boundary regions. However, in contrast to W-1, the bulk hardness of Rx 91 was less than the individual hardness values for the matrix and the grain boundary regions.

For Super Star, two peaks in hardness were observed at annealing temperatures of approximately 500° and 650°C, as shown in Fig. 1 (c). The lower-temperature peak was associated with the grain boundary regions, and the higher-temperature peak was associated with the matrix phase. The bulk alloy hardness was generally almost the same as the matrix phase and much less than the hardness of the grain boundary regions.

3.2 SEM microstructural observations

No obvious microstructural differences were observed for the W-1 specimens annealed at the different temperatures. Typical microstructures are shown in Fig. 2 for a specimen annealed at 922°C. Figure 2 (a) shows the dendritic microstructure of this alloy, with a small amount of porosity in the white-appearing interdendritic regions that are the last portions of the alloy to undergo solidification. The complex multi-phase structure of an interdendritic region is shown in Fig. 2 (b).

Figure 3 (a) shows the microstructure of Rx 91 after annealing at 409°C. Equiaxed palladium solid solution grains can be seen, some of which appear to have a fine-scale etched substructure, but there is no general pattern of large precipitates within these grains. Elongated, narrow precipitates exist at the grain boundaries and are more evident at higher SEM magnification. Porosity can be seen at triple-point grain boundary junctions, as well as along a grain boundary and within one grain. Figure 3 (b) shows the microstructure after annealing at 652°C, where the highest bulk hardness was found. Very small precipitates can be observed in both the matrix and grain boundary regions, along with submicron porosity in the center of the figure. Figure 3 (c) shows that after annealing at 947°C, discontinuous precipitates appeared at the grain boundaries, and the fine-scale precipitates in the matrix have grown. The cube-shaped morphology of these precipitates is shown more clearly in Fig. 3 (d). Using our previously described procedures for the study of ordered phases

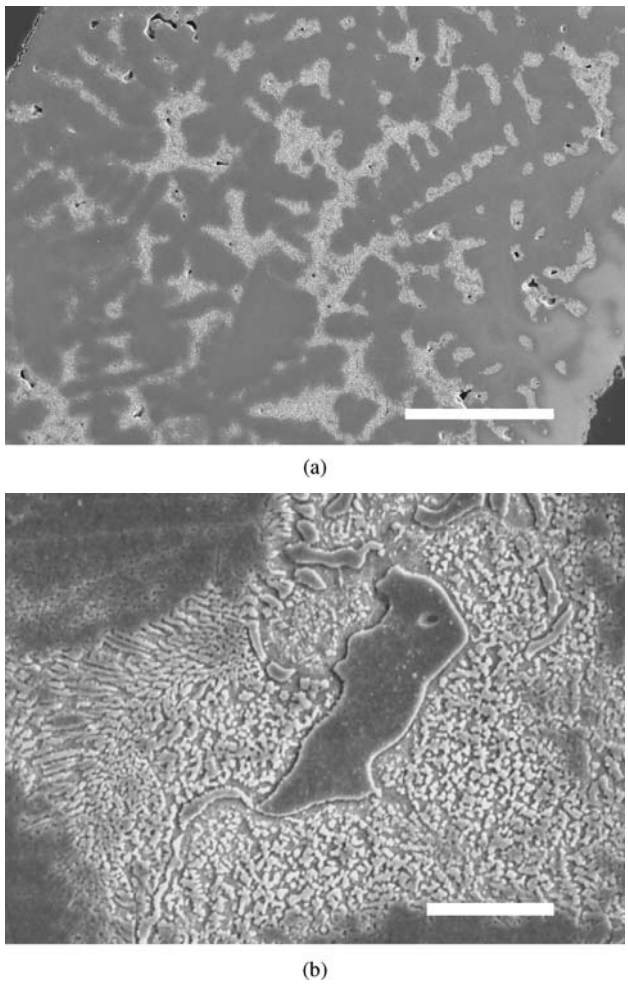

Fig. 2 (a) SEM photomicrograph showing dendritic structure of W-1 annealed at 922°C. (b) Higher-magnification photomicrograph of interdendritic region, showing a multi-phase structure. Length of scale bar = 150 μm for (a) and 5 μm for (b).

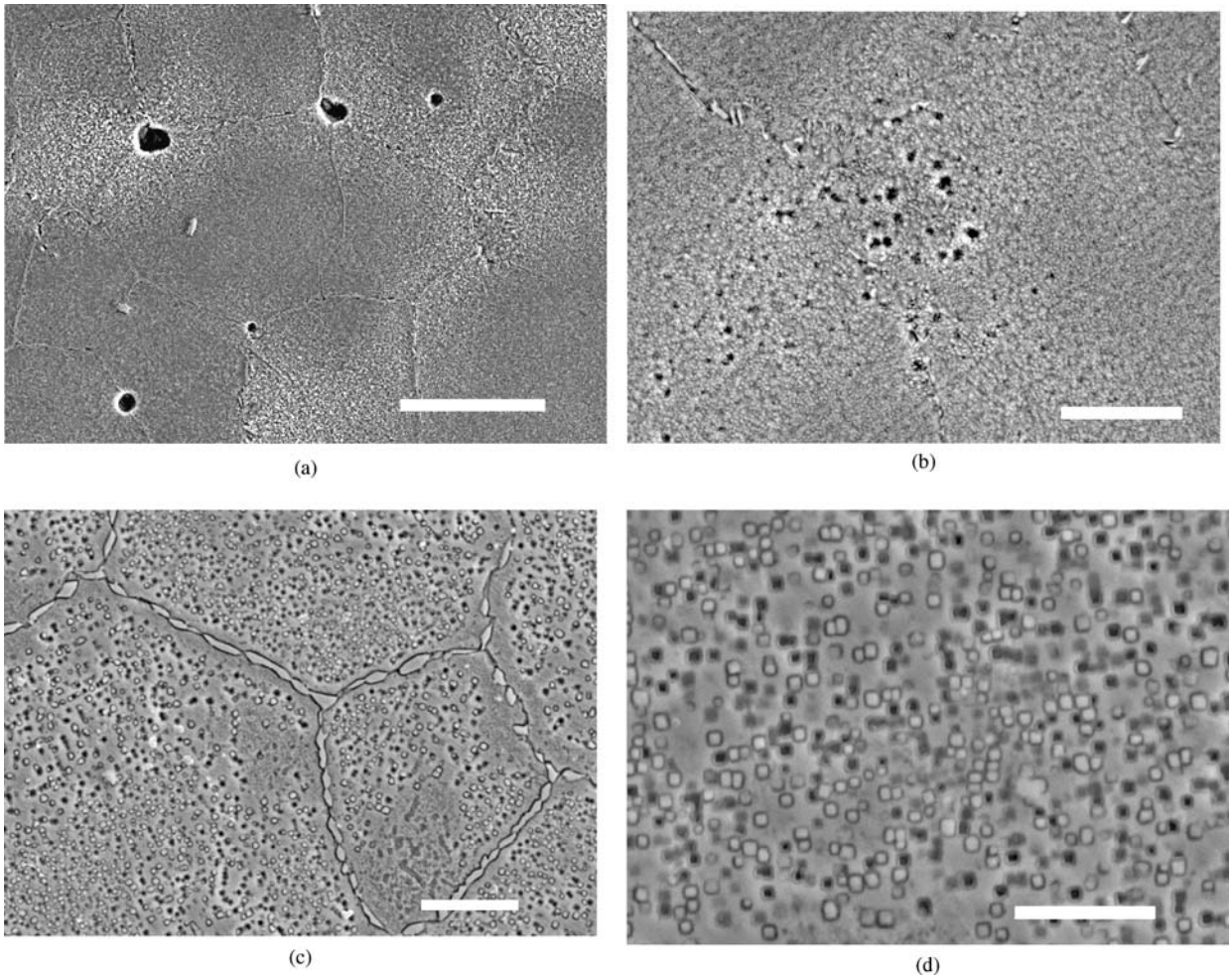

Fig. 3 Secondary electron images of Rx 91: (a) annealed at 409°C, showing equiaxed grains with substructure, grain boundary precipitates, and casting porosity. (b) annealed at 652°C, showing fine-scale porosity and precipitates in matrix and grain boundaries. (c) annealed at 947°C, showing discontinuous precipitates in grain boundaries and adjacent matrix regions denuded of precipitates. (d) higher-magnification photomicrograph of cube-shaped precipitates in matrix. Length of scale bar = 15 μm for (a), 5 μm for (b) and (c), and 3 μm for (d).

in Super Star [11], transmission electron microscopic (TEM) examination has shown that these cube-shaped precipitates in Rx 91 are also ordered. Figure 3 (c) shows that denuded regions exist near the discontinuous precipitates at the grain boundaries, within which the cube-shaped precipitates in the matrix are absent.

Figures 4–6 present photomicrographs of Super Star annealed at several temperatures based upon Fig. 1 (c). Figure 4 (a) is a secondary electron image of the microstructures after annealing at 417°C where the bulk alloy hardness was less than its maximum value. Wide multi-phase regions adjacent to the grain boundaries and grain boundary precipitates are evident. The corresponding backscattered electron image in Fig. 4 (b) shows the lower mean atomic number of the multi-phase regions adjacent to the grain boundaries, compared to the palladium solid solution matrix in the central portions of the grains. Figure 5 (a) and (b) show microstructures after annealing at 512°C where the first hardness peak in Fig. 1 (c) appeared. The matrix phase has more distinct boundaries, and the grain boundary structure appears to be more complex. The multi-phase regions adjacent to the palladium solid solution in the centers of grains have also become more uniform. Figure 6 (a) presents the microstructure after annealing at 561°C, where the bulk alloy hardness has decreased. The regions containing the grain boundary precipitates have become narrower, and the widths of adjacent multi-phase regions have increased. The microstructure after annealing at 662°C, where the bulk hardness is a maximum, is presented in Fig. 6 (b) and shows further increase in the complexity and width of the multi-phase regions adjacent to the grain boundaries, along with evidence of fine-scale precipitation in the matrix. After annealing at 947°C, which causes a decrease in bulk hardness, the microstructure shown in Fig. 6 (c) contains needle-like (acicular) precipitates, as well as discontinuous precipitates in both the matrix and grain boundaries. Residual dendrites in the microstructure, which can be observed in photomicrographs obtained after annealing at lower temperatures, have disappeared.

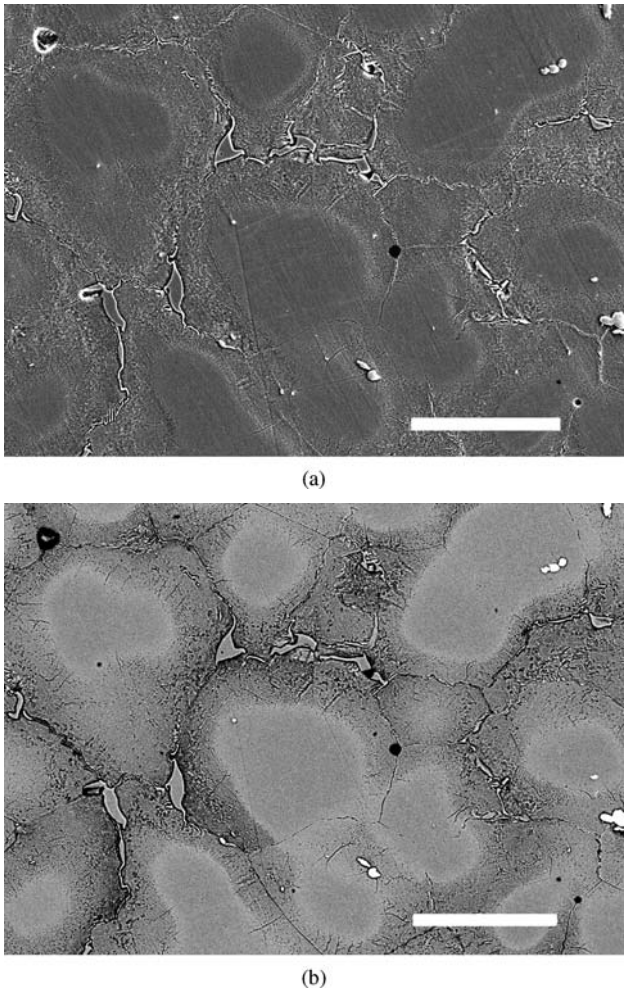

Fig. 4 SEM photomicrographs of Super Star annealed at 417°C, showing highly segregated microstructures: (a) secondary electron image; (b) backscattered electron image. Length of scale bar = 30 μm.

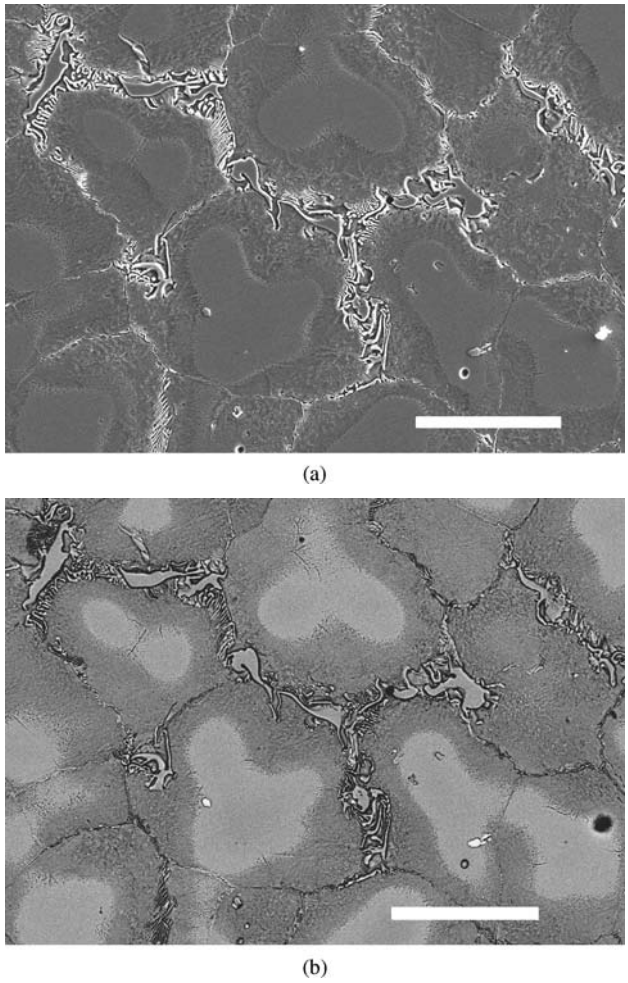

Fig. 5 SEM photomicrographs of Super Star annealed at 512°C: (a) secondary electron image; (b) backscattered electron image. Some redistribution of component elements has taken place, compared to Fig. 4. Length of scale bar = 30 μm.

4 Discussion

Annealing investigations [15–17] have been performed on noble dental alloys other than Pd–Ag alloys because phase transformations exist that cause substantial strengthening and potentially result in improved clinical performance. Since Pd–Ag binary alloys form a simple solid solution system without further solid state reactions [18], any phase transformations during annealing would necessarily involve the solute elements, Sn and In, which have important roles in Pd–Ag dental alloys for porcelain adherence and contribute to alloy castability [3]. The roles of Sn and In for formation of secondary microstructural phases were evident in our recent TEM study of the Super Star alloy [11].

Vickers hardness measurements presented in Fig. 1 indicate that the bulk hardness of the W-1, Rx 91, and Super Star Pd–Ag alloys varied substantially during isothermal annealing. Comparison of the hardness changes of each bulk alloy, with hardness changes in the palladium solid solution matrix and in the other major microstructural constituent, has shown that the dominant precipitation process occurs in the matrix phase. While SEM observations of the annealed Pd–Ag alloys (Figs. 2–6) provide considerable detail about their microstructures, study of the fundamental nature of relevant strengthening mechanisms requires TEM examination of deformed alloys that have been loaded in both uniaxial tension and cyclic fatigue. Such studies have been performed on high-palladium dental alloys [19, 20], and will be reported in a future article for the three Pd–Ag alloys selected for this study.

Although Table 1 shows that there are no large compositional differences for these three Pd–Ag alloys, their microstructures have notable differences. As-cast Super Star has a nearly equiaxed grain structure with extensive microsegregation, some residual dendrites and a fine-scale grain-boundary eutectic structure. This multi-phase microstructure becomes substantially homogenized after the firing cycles for dental porcelain [10, 11]. As-cast Rx 91 has an equiaxed grain structure with minimal microsegregation and no residual

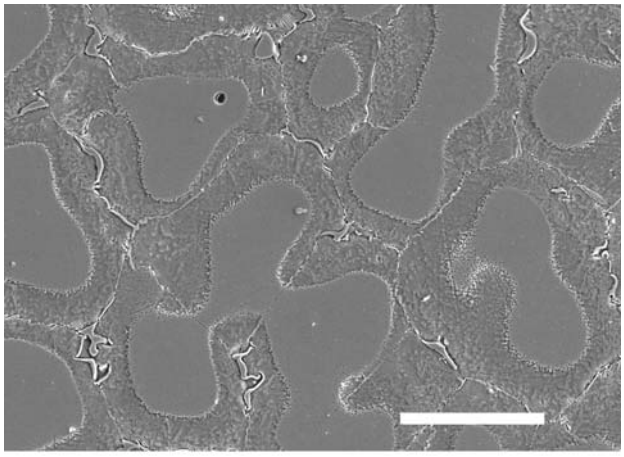

(a)

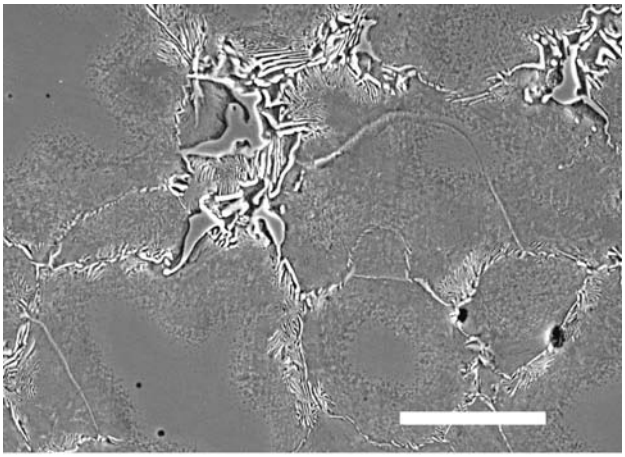

(b)

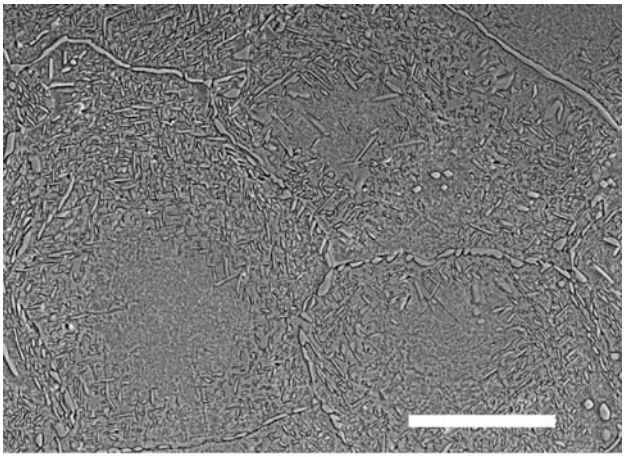

(c)

Fig. 6 SEM photomicrographs of Super Star annealed at: (a) 561°C; (b) 662°C; (c) 947°C. Needle-like precipitates and discontinuous precipitates appeared after annealing at 947°C. Length of scale bar = 30 μm for (a), 10 μm for (b), and 15 μm for (c).

dendrites while as-cast W-1, which has a very similar composition (Table 1), has a dendritic microstructure. (The value of 0.2% yield strength reported by the manufacturer is much higher for Rx 91 compared to W-1.) Microstructural differences for these two alloys are attributed to the proportions of In and Sn, the amounts or absence of refractory grain refinement elements such as Ru and Re [21, 22], and other proprietary alloying strategies such as the use of Li (Table 1).

The precipitation processes that caused hardness changes in the three commercial Pd–Ag alloys (Fig. 1) were not due to formation of internal In and Sn oxides, as suggested by Payan *et al.* [13], for their air-annealing of an experimental Pd–Ag alloy of similar composition, since the present annealing was performed in a nitrogen atmosphere. Both the present and Payan *et al.* [13] studies found that the major precipitation process for increased hardening of the Pd–Ag alloys studied occurs at approximately 650°C.

For W-1, high-temperature annealing at 922°C (approximate upper-temperature limit of porcelain firing cycles) could not convert the dendrites in the as-cast alloy to equiaxed grains. The fine-scale microstructure did not permit identification at the SEM level of precipitates in the matrix phase that were responsible for hardness changes during annealing. For Rx 91, the cube-shaped precipitates in the matrix that were responsible for the hardening were readily observed with the SEM, and growth of these precipitates at higher temperatures (overaging) accounts for the decrease in hardness. Growth of discontinuous precipitates in the grain boundaries at the highest annealing temperature required solute elements that were needed for formation of the cube-shaped precipitates, accounting for the adjacent regions that were denuded of the latter precipitates. For Super Star, comparison of microstructures of specimens annealed at 407° and 512°C, where the first hardening peak occurred, reveals the occurrence of some elemental diffusion to improve the microstructural homogeneity, but no obvious precipitation processes in the multiphase regions outside of the matrix phase could be identified because of the limited SEM resolution. These precipitation processes have been studied by TEM and will be reported in our subsequent publication.

5 Conclusions

Based upon Vickers hardness measurements and SEM observations of three commercial Pd–Ag alloys (W-1, Rx 91 and Super Star), the following conclusions can be drawn:

1. For all three alloys, the dominant change in bulk hardness during annealing between temperatures of approximately 400° to 950°C was due to precipitation in the palladium solid solution matrix phase. The highest Vickers hardness occurred at approximately 700°C for W-1 and 650°C for Rx 91. For Super Star, there were two peaks at approximately 500° and 650°C, with the lower-temperature peak controlled by multi-phase regions adjacent to the matrix grains and the higher-temperature peak by the matrix phase.
2. Although the W-1 and Rx 91 alloys have very similar compositions, the former has a dendritic as-cast microstructure and the latter has an as-cast microstructure with equiaxed grains. Possible reasons for these different microstructures are the proportions of In and Sn in the alloy compositions, the absence or presence of grain refinement elements, and the use of other proprietary strategies by the manufacturers.
3. The needle-like precipitates and the discontinuous precipitates that form in Super Star at the highest annealing temperature cause a reduction in hardness. This annealing temperature and the 30 min annealing time are sufficient to eliminate the residual dendrites present in the as-cast alloy.
4. Detailed understanding of the precipitation processes that occur during annealing these Pd–Ag alloys requires the use of transmission electron microscopy.

Acknowledgments This research was supported by Grant DE10147 from the National Institute of Dental and Craniofacial Research of the National Institutes of Health, Bethesda, MD, USA.

References

1. E. F. HUGET and S. CIVJAN, *J. Am. Dent. Assoc.* **89** (1974) 383.
2. C. J. GOODACRE, *J. Prosthet. Dent.* **62** (1989) 34.
3. R. L. BERTOLOTTI, In: W.J. O'BRIEN (editor), "Dental Materials and Their Selection", 3rd edn (Quintessence, Chicago, 2002), Chap. 14.
4. P. R. MEZGER, A. L. H. STOLS, M. M. A. VRIJHOEF and E. H. GREENER, *J. Dent.* **17** (1989) 90.
5. E. PAPAZOGLOU and W. A. BRANTLEY, *Dent. Mater.* **14** (1998) 112.
6. T. R. WALTON and W. J. O'BRIEN, *J. Dent. Res.* **64** (1985) 476.
7. P. R. MEZGER, M. M. A. VRIJHOEF and E. H. GREENER, *Dent. Mater.* **5** (1989) 97.
8. L. BLANCO-DALMAU, *J. Prosthet. Dent.* **50** (1983) 865.
9. W. J. O'BRIEN, K M. BOENKE, J B. LINGER and C. L. GROH, **14** (1998) 365.
10. S. G. VERMILYEA, Z. CAI, W. A. BRANTLEY and J. C. MITCHELL, *J. Prosthodont.* **5** (1996) 288.
11. W. H. GUO, W. A. BRANTLEY, W. A .T. CLARK, P. MONAGHAN and M. J. MILLS, *Biomaterials* **24** (2003) 1705.
12. J. R. MACKERT Jr, R. D. RINGLE and C. W. FAIRHURST, *J. Dent. Res.* **62** (1983) 1229.
13. J. PAYAN, G. E. MOYA, J. M. MEYER and F. MOYA, *J. Oral Rehabil.* **13** (1986) 329.
14. A. B. CARR and W. A. BRANTLEY, *Int. J. Prosthodont.* **4** (1991) 265.
15. L. NIEMI and H. HERØ, *J. Dent. Res.* **63** (1984) 149.
16. T. TANI, K. UDOH, K. YASUDA, G. VAN TENDELOO and J. VAN LANDUYT, *J. Dent. Res.* **70** (1991) 1350.
17. I. WATANABE, E. WATANABE, Z. CAI, T. OKABE and M. ATSUTA, *Dent. Mater.* **17** (2001) 388.
18. T. B. MASSALSKI (editor-in-chief), "Binary Alloy Phase Diagrams", **1–2** (American Society for Metals, Metals Park, OH, USA, 1986) 34, 71, 1390, 1874.
19. W. H. GUO, W. A. BRANTLEY, W. A. T. CLARK, J. Z. XIAO and E. PAPAZOGLOU. *Dent. Mater.* **19** (2003) 334.
20. W. H. GUO, W. A. BRANTLEY, D. LI, P. MONAGHAN and W. A. T. CLARK. *J. Mater. Sci.: Mater. Med.* **13** (2002) 369.
21. J. P. NIELSEN and J. J. TUCCILLO, *J. Dent. Res.* **45** (1966) 964.
22. W. A. BRANTLEY, Z. CAI, A. B. CARR and J. C. MITCHELL, *Cells Mater.* **3** (1993) 103.